Journal of Sound and Vibration (2001) **245**(2), 217–237
doi:10.1006/jsvi.2001.3575, available online at http://www.idealibrary.com on IDEAL®

NOISE GENERATION OF BLADE–VORTEX RESONANCE

R. C. K. Leung† and R. M. C. So

Department of Mechanical Engineering, The Hong Kong Polytechnic University, Hung Hom, Kowloon, Hong Kong, People's Republic of China. E-mail: rckleung@copeland-corp.com

(*Received* 4 *October* 2000)

A numerical study of the aerodynamic noise generated when an airfoil/blade in a uniform flow is excited by an oncoming vortical flow is reported. The vortical flow is modelled by a series of flow convected discrete vortices representative of a Karman vortex street. Such noise generation problems due to fluid–blade interaction occur in helicopter rotor and turbomachinery blades. Interactions with both rigid and elastic airfoil/blade are considered. Under a vortical excitation, aerodynamic resonance of the airfoil/blade at certain excitation frequencies is found to occur and loading noise is generated due to the fluctuations of the aerodynamic loading on the airfoil/blade. For an elastic blade, due the occurrence of structural resonance incited by the flow-induced vibration of the airfoil/blade, a stronger loading noise is generated. The associated thickness effect due to the airfoil/blade vibration is extremely weak. The magnitude of the noise was found to depend on the frequency of the oncoming vortical flow and the geometry and rigidity of the blade.

1. INTRODUCTION

Fluid–structure interactions can be found in a variety of engineering applications where the system considered or some of its components are either directly in contact with or completely immersed in a flowing fluid. Examples of this situation are blades in turbomachines, heat exchanger tubes exposed to coolant cross-flow, tube bundles in nuclear and chemical reactors, bundles of overhead transmission lines or chimney stacks subject to atmospheric winds, helicopter rotor blades interacting with their own wakes, etc. The unsteady aerodynamics induces unsteady forces on the structural components and, if the structure is elastic, the interactions are further complicated by the fact that the structural response could modify the flow field. Under certain unfavorable conditions, the vibratory structural response could create unfavorable operating conditions that could lead to catastrophic structural failure [1, 2]. In some cases, it would also create annoying noise to the people working or residing around. Among the various forms of fluid–structure interactions investigated, the vortex–body interaction and its noise generation have attracted most attention since it is rather simple to handle but still covers the majority of the underlying flow physics.

Impulsive noise generation by the interaction of helicopter rotor blades with concentrated tip vortices shed from preceding blades is one of the major sources of helicopter noise. When these shed vortices interact with the trailing rotor blades, the unsteady pressure fluctuations induced on the blade surfaces would lead to severe dynamic

† Presently affiliated with Asia Pacific Engineering Center, Copeland Corporation, Kwun Tong, Kowloon, Hong Kong.

0022-460X/01/320217 + 21 $35.00/0

structural loading and noise generation. The blade–vortex interaction noise (BVI) is a major source of the so-called blade slap noise of helicopters, which commonly occurs in descent flight. Analytical study by Widnall [3] arrives at a conclusion that the parallel blade–vortex interaction generates the strongest pulse in the helicopter noise spectrum. The conclusion was later confirmed by the noise source identification study of Splettstoesser *et al.* [4]. Therefore, the helicopter BVI noise has been commonly studied in the form of a two-dimensional parallel interaction noise problem, for instance references [5–8].

When a discrete vortex passes over a rigid airfoil, the aerodynamic forces on the airfoil vary and noise is generated as a result. The magnitude of the noise depends on the circulation of the vortex and the transverse spacing between the vortex and the blade. However, the discrete vortex representation of the upstream vortical excitation encountered by the blade is far from reality. Under different flight conditions, the helicopter blades may be twisted to control the lift and consequently alternating vortices are shed from the blade. Poling *et al.* [9] studied the pressure distributions of the BVI of the helicopter blade by modeling it as a rigid blade immersed in a finite sequence of alternating vortices. Good agreement with experimental results is obtained. However, the noise generation due to such a BVI is not addressed.

In a turbomachinery environment, each blade row in a multistage turbomachine generates vortical wakes that are convected into the downstream blade row. When a turbulent wake or a vortex approaches a downstream structure, be it rigid or elastic, the structure could be agitated to radiate noise [8, 10] and this form of excitation could be an efficient noise source. This situation could present another potential element contributing to structural failure. The flow-induced noise generated from structures may excite the acoustic resonance of the surrounding flow cavity or blade cascade [11, 12]. This phenomenon occurs when the aerodynamic forcing due to vortex shedding from blades synchronizes with the resonant frequency of the cavity volume. The noise pressure grows rapidly and strengthens the unsteady excitation of the structures, which feeds back to excite the noise-generating vortex shedding from the blades. Eventually, the excitation could lead to premature structural failure of the blades [13]. This situation has to be avoided for proper functioning of turbomachines. Due to the complexity of the surrounding cavity geometry, such flow-induced noise problems are more conveniently tackled at the source level so that an understanding of the mechanism of noise generation from the vibrating blades is essential.

The flow in the blade passage of turbomachines is usually turbulent and the associated Reynolds number is extremely high. If the co-ordinates are fixed with respect to the downstream blade row, the oncoming turbulent mean flow with the convected vortices generated by the upstream blades would appear to be unsteady and the fluid–structure interactions associated with the blades are very complicated [14]. Recently, the flow-induced vibrations of an airfoil/blade due to periodic oncoming vortices have been studied by So *et al.* [15] in an attempt to assess the fatigue life of turbine blades. They found that the fluctuations of the loading of the rigid blades follow the oncoming excitation and attain peak values at certain excitation frequencies. This phenomenon is termed aerodynamic resonance. If the blade is elastic, the structural response would make the entire fluid–blade system resonate at different excitation frequencies, leading to the occurrence of structural resonance. However, they did not study the acoustic response of the resonance of such a blade–vortex interaction.

The present paper extends the work of So *et al.* [15] and concentrates on the noise generation due to the aerodynamic resonance and structural resonance of a blade excited by an oncoming vortical flow. In the case of helicopter rotor and turbomachinery blades, the vortical flow is given by the oncoming vortices generated, respectively, by the turbulent flow

around the preceding rotor blade and by the upstream blade row. These vortices are shed from the upstream in an alternating manner with a wide range of frequencies. As a first attempt, a finite number of frequency components are considered. In this way, the techniques developed by Jadic *et al.* [16] and So *et al.* [15] are directly applicable.

2. COUPLED BLADE–VORTEX DYNAMICS

The fully coupled blade–vortex interaction problem is resolved by the methodology proposed by Jadic *et al.* [16] and So *et al.* [15]. In the present study, the main interest is in the aerodynamic and acoustic response of the blade due to an upstream source of vorticity, which may be approximated by isolated vortices in a prescribed pattern of approach. According to Crighton [17], in low Mach number source flow, the viscous effect radiates an extremely inefficient octupole noise and its contributions to the far field noise can be ignored. Therefore, as a first approximation, viscous effect is neglected and the whole flow field is considered inviscid. In view of this, the unsteady flow is assumed to be incompressible, two-dimensional and governed by the Euler equations. The transport equation for the vorticity $\boldsymbol{\omega} = \mathbf{V} \times \mathbf{V}$ can be deduced by taking the curl of the Euler equation. The circulation Γ around a given material curve in the flow field is supposed to remain unchanged during each time step δt. Consistent with this approach, it is also assumed that, during each time step δt, the vorticity is essentially frozen and is convected by the inviscid flow. Mathematically, this assumption can be written as

$$\mathbf{x}_i(t + \delta t) = \mathbf{x}(t) + \mathbf{V}_0(\mathbf{x}_i(t), \omega_i(t), t)\, \delta t, \quad i = 1, 2, \ldots, N, \tag{1}$$

where $\omega_i(t)$ and $\mathbf{x}_i(t)$ are the strength and the position vector of the ith vortical element, N is the number of vortical elements at time t and $\mathbf{V}_0$ denotes the convective velocity generated by the inviscid flow. The set of equations (1) is in fact an explicit finite difference form of the differential set of equations which relate/track the position of a certain vortical element to the velocity of the inviscid flow at that particular position. The flow around the blade, which is simulated by a distribution of sources and discrete vortices, is solved using a boundary element method for inviscid incompressible flows. In the boundary element formulation, unsteady Kutta condition at the trailing edge of the blade is imposed to accurately determine the vorticity distribution at the edge [16]. The tangency condition, i.e $(\mathbf{V}_0 - \mathbf{V}_s) \cdot \mathbf{n} = 0$ where $\mathbf{V}_s$ is the velocity of the blade surface, is applied on the blade surface. The far field boundary condition is given by $\mathbf{V}_0 = U_\infty \hat{\mathbf{e}}_{y1} + \mathbf{V}_\omega$, where $\mathbf{V}_\omega$ is the rotational part of $\mathbf{V}_0$ and $\hat{\mathbf{e}}_{y1}$ is the unit vector along the streamwise direction y_1. The flow over the blade remains attached and a free wake model is assumed for the wake. For further details on the formulation of the aerodynamics, readers are referred to Jadic *et al.* [16] and So *et al.* [15]. Once the velocity and pressure fields are known, the unsteady forces and moments on the blade can be determined by integrating around the blade.

The structural dynamic response of the blade is governed by a set of partial differential equations if its mass is continuously distributed, and/or ordinary differential equations if its mass is approximated by lumped masses. Although these equations are often assumed to be linear, non-linearity may appear due to geometric factors, e.g., large blade rotations, intermittent contact of shrouds, etc., or to the blade material properties such as material yielding or plastic behavior. In the context of airfoils or turbomachinary blades, a simple two-degree-of-freedom model can be assumed to account for the non-linear effects. Thus, the equations of the blade motion are

$$m\ddot{h} - ma\cos\theta\,\ddot{\theta} + K_h h + ma\sin\theta\,\dot{\theta}^2 = L, \tag{2}$$

$$I\ddot{\theta} - ma\cos\theta\,\ddot{h} + K_\theta = M, \tag{3}$$

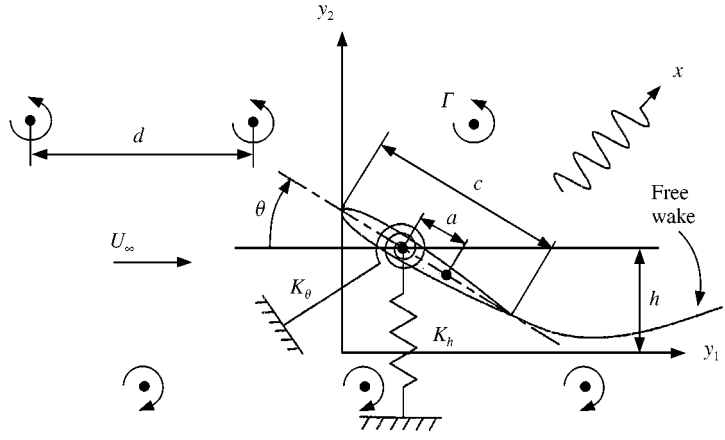

Figure 1. An idealized problem of blade–vortex interaction and noise generation.

where h is the plunging displacement of the blade, which models the bending deformations, and θ is the pitching angle of the blade, which models the torsional deformations. The coefficient a is the distance between the elastic axis and the center of mass (Figure 1). The mass of the blade section per unit length in the spanwise y_3 direction is denoted by m, and I is the moment of inertia of the blade section. The coefficients, K_h and K_θ, are the bending and torsional stiffness of the blade and the aerodynamic lift and moment acting on the blade are designed by L and M respectively.

The flow over the blade and its structural response are coupled to each other through the no-slip or tangency boundary condition, which accounts for the effect of structural response on the blade flow, and the aerodynamic forces which account for the effect of the blade flow on the structural response. In the present study, the flow field is required to satisfy, at every point of the blade surface in contact with the fluid, the tangency condition, $(\mathbf{V}_0 - \mathbf{V}_s)\cdot \mathbf{n} = 0$. Here, $\mathbf{V}_0$ and $\mathbf{V}_s$ are the local velocities of the fluid and the blade, respectively, and $\mathbf{n}$ is the local outward normal to the contact surface. This boundary condition is in general non-linear since both the velocities and the direction of the normal depend on either the flow field variables or the structural response. The flow affects the structural response through the aerodynamic forces L and M exerted on the blade, equations (2) and (3). The force and moment on the blade can be evaluated from

$$C_p = \frac{p - p_\infty}{\rho_0 U_\infty^2/2} = \left(-2\frac{\partial \phi}{\partial t} + V_b^2 - V_T^2 \right)\frac{1}{U_\infty^2}, \tag{4}$$

where p is the hydrodynamic pressure on the blade surface, p_∞ is the freestream reference pressure, ρ_0 is the fluid density, V_b is the velocity induced by the freestream and blade surface motion, V_T is the velocity induced by the source and vorticity distributions bounded on the blade surface, the freely convecting vortices and the wake vortices. The aerodynamic lift and moment appearing in equations (2) and (3) can then be evaluated from the following relations:

$$C_L = -\oint [-C_p(\gamma) n_{y1} \sin\alpha + C_p(\gamma) n_{y2} \cos\alpha]\, \mathrm{d}\gamma, \tag{5}$$

$$C_M = \oint \{[y_1(\gamma) - y_{1p}] C_P(\gamma) n_{y2} - [y_2(\gamma) - y_{2p}] C_P(\gamma) n_{y1}\}\, \mathrm{d}\gamma, \tag{6}$$

where γ is the arc length of the blade surface profile, n_{y1} and n_{y2} are components of the outward normal in y_1 and y_2 respectively; the position of the blade mass center is (y_{1p}, y_{2p}) and α is the angle of attack.

3. FARFIELD NOISE GENERATION

The governing equation of the noise generated by the unsteady flow in the presence of an impenetrable blade in arbitrary motion to a far field observer at $\mathbf{x} = (x_1, x_2, x_3)$ in ambient is the Ffowcs Williams–Hawkings (FW–H) equation [18] which may be written in differential form as

$$\left(\frac{1}{c_0^2}\frac{\partial^2}{\partial t^2} - \nabla^2\right) p'(\mathbf{x}, t) = \frac{\partial}{\partial t}[\rho_0 v_n \delta(f)] - \frac{\partial}{\partial x_i}[L_i \delta(f)] + \frac{\partial^2}{\partial x_i \partial x_j}[T_{ij} H(f)], \tag{7}$$

where c_0 is the ambient speed of sound, t is the observer time, $p' \equiv \rho' c_0^2$ is the acoustic pressure, ρ' is the density perturbation, $T_{ij} = \rho u_i u_j + P_{ij} - c_0^2 \rho' \delta_{ij}$ is the Lighthill stress tensor with P_{ij} as the compressive stress tensor, $L_i = P_{ij}\mathbf{n}_j$. The blade surface is described by the equation $f(\mathbf{y}, t) = 0$ with $\mathbf{y} = (y_1, y_2, y_3)$ and $\delta(f)$ and $H(f)$ are the Dirac delta and Heaviside functions respectively. In the aeroacoustics literature, the three source terms on the right-hand side of equation (7) are, respectively, known as the thickness, loading and quadrupole sources [18].

An integral representation of the solution to equation (7) may be obtained by utilizing the formulation due to Farassat and his co-workers [19, 20], which can be written as

$$p'(\mathbf{x}, t) = p'_T(\mathbf{x}, t) + p'_L(\mathbf{x}, t) + p'_Q(\mathbf{x}, t), \tag{8}$$

$$p'_T(\mathbf{x}, t) = \frac{1}{4\pi}\int_{f=0}\left[\frac{\rho_0(\dot{v}_n + v_{\dot{n}})}{R(1 - M_R)^2}\right]_{ret} \mathrm{d}S + \frac{1}{4\pi}\int_{f=0}\left[\frac{\rho_0 v_n (R\dot{M}_R + c_0(M_R - M^2))}{R^2(1 - M_R)^3}\right]_{ret} \mathrm{d}S, \tag{9}$$

$$p'_L(\mathbf{x}, t) = \frac{1}{4\pi\tau_0}\int_{f=0}\left[\frac{\dot{L}_R}{R(1 - M_R)^2}\right]_{ret} \mathrm{d}S + \frac{1}{4\pi}\int_{f=0}\left[\frac{L_R - L_M}{R^2(1 - M_R)^2}\right]_{ret} \mathrm{d}S$$

$$\frac{1}{4\pi\tau_0}\int_{f=0}\left[\frac{L_R(R\dot{M}_R + c_0(M_R - M^2)}{R^2(1 - M_R)^3}\right]_{ret} \mathrm{d}S, \tag{10}$$

and $\mathrm{d}S$ is an elemental area on the blade surface $f = 0$, $R = |\mathbf{x} - \mathbf{y}|$ is the distance between the source and observer points, p'_T and p'_L are the thickness and loading noise respectively. In equations (9) and (10), $L_R = L_i R_i$ is the component in the radiation direction of the local lift force that acts on the fluid, $L_M = L_i M_i$ is the component of the blade velocity in the local force direction, $v_n = v_i \mathbf{n}_i$ is the local blade surface velocity in the direction normal to $f = 0$, and $M_R = M_i R_i$ is the component of blade velocity in the radiation direction normalized by c_0. The bracket $[\cdots]_{ret}$ means evaluation at the retarded time $\tau = t - R/c_0$ and the dot indicates a retarded time (source time) differentiation (i.e., $\partial/\partial t$). The quadrupole noise p'_Q due to turbulence outside the blade surface is very weak when compared with p'_T and p'_L in the case of subsonic blade velocity [20], and is neglected in the present study. Furthermore, due to the same reason, the last terms in equations (9) and (10) are also neglected.

Equations (9) and (10) are valid for the aerodynamic noise generation from three-dimensional acoustically compact blades. However, for two-dimensional blades, the infinite extent in spanwise y_3 direction would violate the assumption of acoustical compactness and care has to be taken in evaluating the corresponding two-dimensional noise generation.

Writing $\mathrm{d}S = \mathrm{d}\gamma\,\mathrm{d}y_3$, where $\mathrm{d}\gamma$ is an elemental arc length of the blade profile. Ffowcs Williams and Hawkings [21] noticed that as the only dependence of the integrands in equations (9) and (10) on y_3 is through the source time $\tau = t - R/c_0$, the y_3 integration is effectively a time integration. Replacing y_3 by τ as the independent variable and after some algebra, equations (9) and (10) can be approximated in dimensionless form as

$$p'_T \approx \frac{1}{\sqrt{2}\pi\sqrt{M_\infty}\sqrt{r}} \int_{-\infty}^{t-M_\infty r} \left(\Lambda_{T1} + \frac{\Lambda_{T2}}{r}\right) \frac{1}{\sqrt{(t-\tau) - M_\infty r}}\,\mathrm{d}\tau, \tag{11}$$

$$p'_L \approx \frac{\sqrt{M_\infty}}{2\sqrt{2}\pi\sqrt{r}} \int_{-\infty}^{t-M_\infty r} \left(\Lambda_{L1} + \frac{\Lambda_{L2}}{r}\right) \frac{1}{\sqrt{(t-\tau) - M_\infty r}}\,\mathrm{d}\tau, \tag{12}$$

where

$$\Lambda_{T1}(\tau) = \int_\gamma (\dot{v}_n + v_{\dot{n}} + M_\infty v_n \dot{v}_r)\,\mathrm{d}\gamma,$$

$$\Lambda_{T2}(\tau) = \int_\gamma v_n (v_r - M_\infty v^2)\,\mathrm{d}\gamma,$$

$$\Lambda_{L1}(\tau) = \int_\gamma (\dot{C}_p + M_\infty C_p \dot{v}_r)\, n_r \mathrm{d}\gamma,$$

$$\Lambda_{L2}(\tau) = \int_\gamma C_P\,[(M_\infty^{-1} + v_r - M_\infty v^2)\, n_r - v_n]\,\mathrm{d}\gamma.$$

For clarity, the prime for all dimensionless variables is dropped in the above equations. Here $\mathbf{r}$ is the two-dimensional position vector of the farfield observer in the y_1y_2 plane and $r = \sqrt{(x_1 - y_1)^2 + (x_2 - y_2)^2}$ is the radiation distance, $M_\infty = U_\infty/c_0$ is the freestream Mach number. It should be noted that the integrands are now independent of y_3. Equations (11) and (12) can then be solved numerically by further substituting $c_0(t - \tau) - r$ by β^2 with the assumption that there is no noise at $\mathbf{x}$ for $t < r/c_0$ [22]. It should be noted that the present study concentrates on the noise generation problem only. The coupling interactions of noise with the aerodynamics of the blade, such as the noise absorption resulting from vortices generated at the trailing edge [23], are not considered.

4. RESULTS AND DISCUSSIONS

4.1. UPSTREAM VORTICAL EXCITATION MODEL

Part of the mechanisms of noise generated by blade–vortex interaction has been investigated previously. For example, former studies [7, 24] focus on the so-called vortex-cutting noise, which is generated when a single discrete vortex impinges, but does not touch, or "cuts", the leading edge of the airfoil. These studies reveal that the major vortex dynamics is responsible for the generation of impulsive noise pulse in the far field but the single discrete vortical disturbance is too simple to model the excitation in real physical situations. In reality, the excitation is generated continuously upstream, like the vortices shed from the blade in the rotary flow of helicopter rotor or the vortices shed from the stator/rotor blade row of an operating turbomachine. The work of Hodson and Dawes [25] demonstrates that the rotational flow through a turbine blade row exhibits features similar to those of a periodic and discrete vortex street. Poling *et al.* [9] employed a discrete vortex model similar to a Karman vortex street (KVS) to describe the upstream vortical excitation

encountered by a helicopter blade, and qualitative agreement in blade aerodynamic response with experiments was achieved. Funazaki and Nishiyama [26] and Feiereisen *et al.* [14] simulated upstream blade row by a set of circular bars, which were moved ahead of the stator row, to investigate the interaction phenomena in turbomachinery.

In the present study, the upstream excitation model encountered by the blade may consist of a series of flow convected vorticity perturbations released from the preceding helicopter rotor blade, or from the upstream blade row in turbomachines. Its excitation pattern may be similar to a KVS pattern, which is modeled by two series of alternating discrete vortices (Figure 1). The freestream velocity is U_∞, the chord length of the blade is c and the spacing of the oncoming vortices is d. Based on these quantities, a frequency parameter, U_∞/d, of the excitation can be defined, which reduces to c/d after normalization of the equations by U_∞ and c. The non-dimensional frequency parameter c/d is used to characterize the upstream excitation throughout this study. In order to assess the influence of blade geometry, two types of blade profiles are investigated, a symmetrical 12% thick NACA 0012 airfoil [27] section and a high-loading T1 blade [14] which is typical in turbine applications. The two blades used have identical chord length c.

The choice of release points for the alternating vortices follows the arguments of So *et al.* [15]. The NACA 0012 airfoil and the T1 blade have completely different aerodynamic loading. Therefore, if a symmetric KVS pattern is used, the T1 blade could find itself lying partially or completely outside of the vortex pattern. The resulting vigorous vortex interactions could give rise to a situation where the blade fails to enter into a time-stationary state. In order to ensure that every released vortex is able to properly interact with the airfoil/blade, an asymmetric release, with two release points located at $y'_1 = -1{\cdot}0$, $y'_2 = 0{\cdot}3$ and $y'_1 = -1{\cdot}0$, $y'_2 = -0{\cdot}2$, is adopted. The released vortices have a normalized strength equal to $\Gamma' = 0{\cdot}1$, corresponding to a lift coefficient of $C_L = 0{\cdot}2$ for the given blades. It should be pointed out that the selection of the locations of the vortex release points is dependent on the value of Γ and the aerodynamic loading character of the blade under consideration.

The number of time steps used in all the computations is 6000 with normalized time step $\delta t' = 0{\cdot}05$. This choice of time step guarantees that the effect of initial conditions decays completely and stationarity in all computed time histories is fully established. The spectral contents of the stationary time histories are then obtained from fast Fourier transform (FFT). In the present study, U_∞ and c are set to 100 m/s and 0·2 m, respectively, for all computations. The characteristic velocity and length scales are assumed to be U_∞ and c. In the following, unless otherwise stated, variables with a prime denote normalized variables. For all computations, the location of the far field observer x is arbitrarily chosen at a radius of 50 chord lengths above the blade.

4.2. NOISE DUE TO AERODYNAMIC RESONANCE

In this section the aerodynamic noise generation due to the interaction of the oncoming KVS excitation with a rigid blade is presented. Within a given vortex release period, when a positive and a negative vortex pass over the rigid blade, the aerodynamic forces and moments acting on the blade will fluctuate under the alternating induction of the oncoming vortices. If the separation of the vortices is small relative to the blade chord, the blade experiences a large number of chordwise aerodynamic fluctuations, which yield a limited response of the blade as a whole since the influences of these fluctuations are averaged off by integration. In the case where the vortex separation is large or comparable to the blade chord, the blade will experience throughout its chord length the same kind of fluctuations.

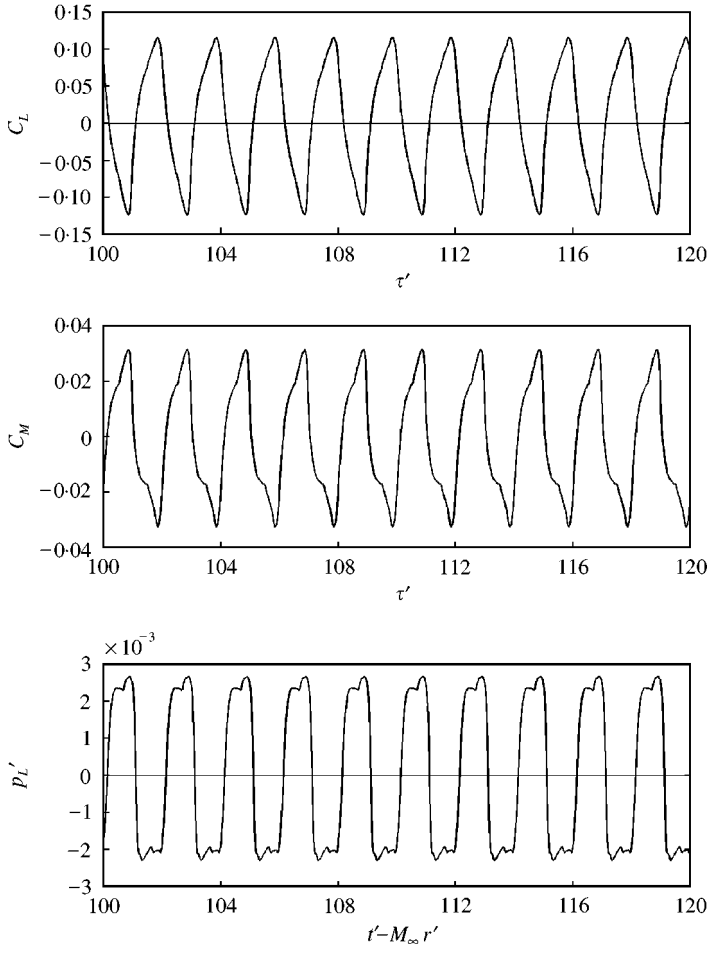

Figure 2. Time histories of the lift coefficient C_L, moment coefficient C_M and loading noise p_L' for the rigid NACA 0012 airfoil with $c/d = 0{\cdot}5$.

There is no averaging effect. As a result, a larger aerodynamic response is experienced by the blade. This argument suggests that the aerodynamic response could reduce as the separation distance d of the oncoming vortice is decreased, i.e., with an increase in the frequency of the oncoming vortical excitation. However, the work of So *et al.* [15] showed that this trend is only partially true for decreasing vortex separation. They demonstrated that the blade–vortex system exhibits an aerodynamic resonance at certain discrete blade chord to vortex separation ratios, c/d, where the blade attains particularly strong aerodynamic response.

The aerodynamic results of So *et al.* [15] are reproduced here to serve as a reference for the noise results. Figures 2 and 3 illustrate the typical time histories of the lift and moment coefficients, C_L and C_M, for the NACA 0012 airfoil and the T1 blade respectively. The frequency parameter c/d of the oncoming vortices is 0·5. It can be seen that the unsteady forces, and thus the aerodynamic coefficients, of the rigid blade resonate with the oncoming vortices and they vary with the same frequency as the oncoming vortices. In fact, the amplitude and pattern of fluctuations depend critically on the frequency parameter c/d. The first harmonic and the root mean square values of C_L, denoted as $(C_L)_{1st}$ and $(C_L)_{r.m.s.}$,

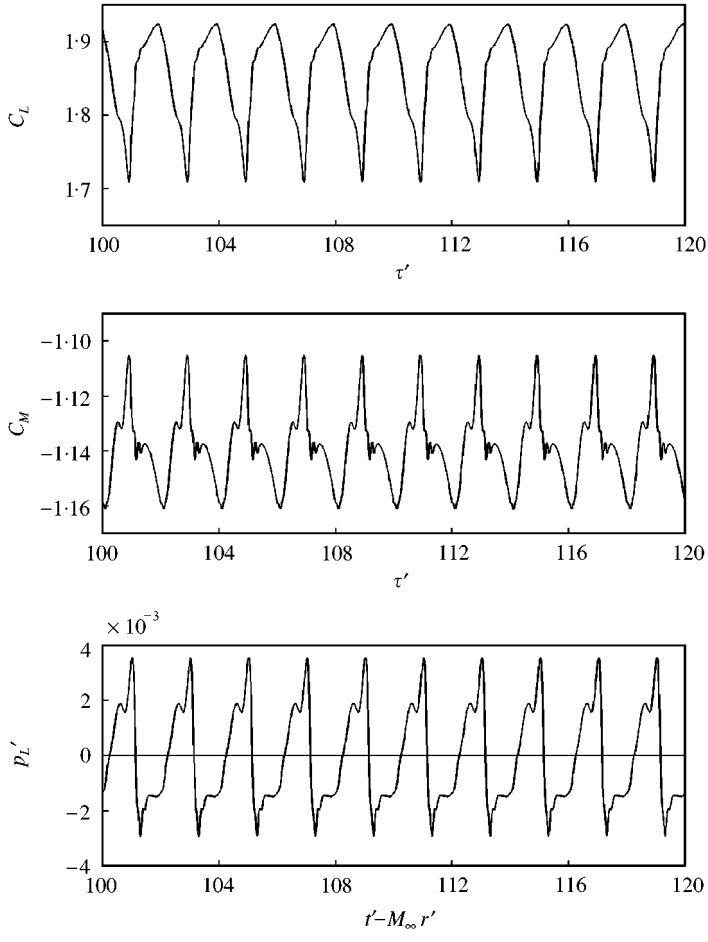

Figure 3. Time histories of the lift coefficient C_L, moment coefficient C_M and loading noise p'_L for the rigid T1 blade with $c/d = 0{\cdot}5$.

respectively, and C_M, denoted as $(C_M)_{1st}$ and $(C_M)_{r.m.s.}$, respectively, of the rigid NACA 0012 airfoil and the T1 blade are computed for a range of frequency parameters covering $0 \leqslant c/d \leqslant 3$ (Figure 4). For both NACA 0012 airfoil and T1 blade, the values of $(C_L)_{1st}$ and $(C_M)_{1st}$ decrease with c/d but dominant peaks can be observed around $c/d = 0{\cdot}5$, $1{\cdot}5$, and $2{\cdot}5$. A similar trend can be observed in the distributions of $(C_L)_{r.m.s.}$ and $(C_M)_{r.m.s.}$. The amplitudes of the dominant peaks decrease with c/d. In the $(C_L)_{1st}$ and $(C_L)_{r.m.s.}$ distributions of the NACA 0012 airfoil, the amplitudes of their second peak range from about 55 to 64% of those of the first peak, while the amplitude of the third peak of $(C_L)_{1st}$ is about 25% of the first peak. The relative amplitudes of the peaks for the T1 blade show a different distribution. The amplitudes of the first and second peaks in both $(C_L)_{1st}$ and $(C_L)_{r.m.s.}$ distributions are comparable and that of the third peak is around 75% of the first peak. This quantitative difference in the peak amplitudes may be attributed to the difference in the loading characteristics of the two blade types. It can be seen that, for both blade types, the amplitudes of the $(C_L)_{1st}$ and $(C_M)_{1st}$ distributions are higher than their corresponding $(C_L)_{r.m.s.}$ and $(C_M)_{r.m.s.}$ distributions, indicating that the first vortical excitation has a significant contribution to the overall aerodynamic response of the blade. Together, these

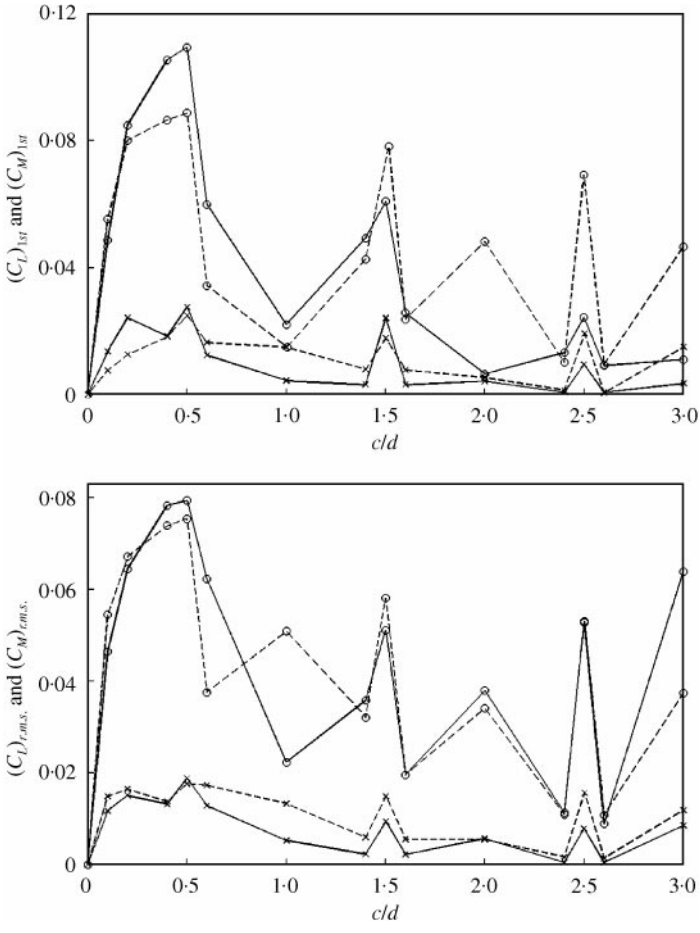

Figure 4. Variations of the first harmonic and root mean square values of the lift and moment coefficients, C_L and C_M, with c/d for rigid blade. ———, NACA 0012 airfoil; – – – – – –, T1 blade. ○, C_L; ×, C_M.

observations demonstrate that there exists an aerodynamic resonance occurring at $c/d = 0{\cdot}5$, 1·5 and 2·5. This phenomenon is purely of aerodynamic origin since the blade is rigid, thus avoiding the possibility of aerodynamic interaction with the blade motion.

According to equation (9), a rigid blade would not generate thickness noise because $\mathbf{v} = 0$; only loading noise p'_L would be detected in the far field. The loading noise p'_L generated from a rigid blade under oncoming KVS excitations is computed and the distributions of the normalized first harmonic and root mean square value, $(p'_L)_{1st}$ and $(p'_L)_{r.m.s.}$, respectively, are shown in Figure 5. The trend of the distributions is similar to those of C_L and C_M (Figure 4). Three distinct peaks appear at $c/d = 0{\cdot}5$, 1·5 and 2·5, showing that the aerodynamic loading on the rigid blade is the major source of noise generation. On the other hand, the noise generation from the T1 blade is in general higher than that from the NACA 0012 airfoil for all values of c/d investigated except at $c/d = 0{\cdot}5$ where the noise generation from both blades is comparable. The higher distributions show that a high loading blade would generate louder noise. In fact, an evident correlation between the noise and the aerodynamic response of the rigid blade can be observed by comparing the time histories of the loading noise and the aerodynamic coefficients, as illustrated in Figures 2 and 3. Note that in these figures, the retarded time, $\tau' = t' - M_\infty r'$, is selected for the noise signature so that it can be

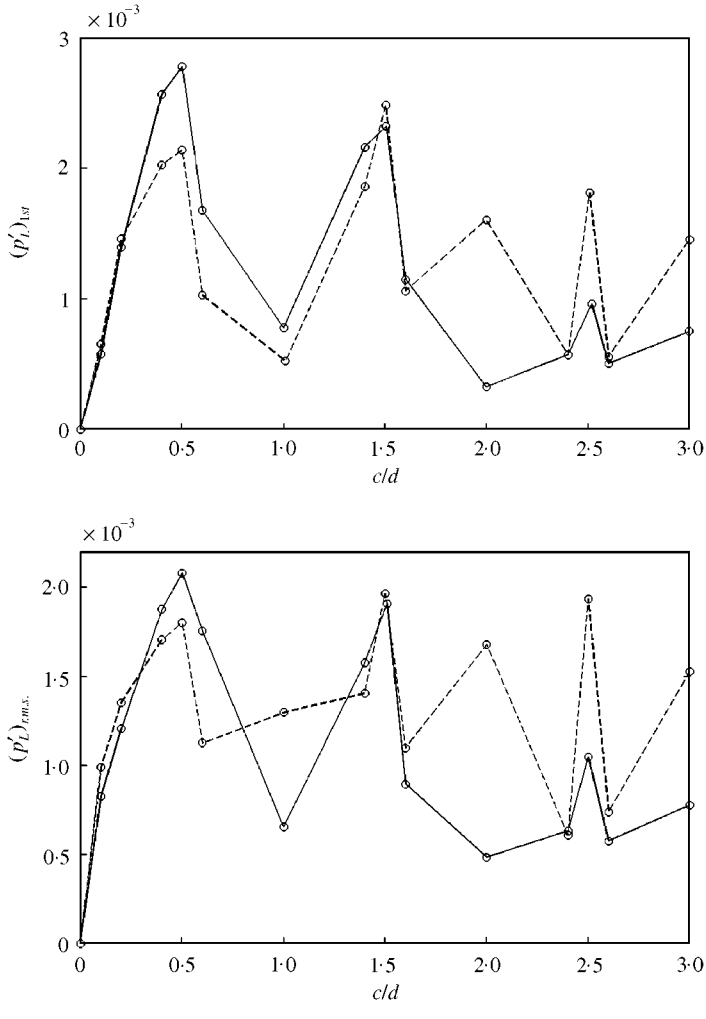

Figure 5. Variations of the first harmonic and root mean square values of the loading noise p'_L with c/d for rigid blade. ———, NACA 0012 airfoil; – – – – – –, T1 blade.

compared with the aerodynamics of the blade on the same time scale. Whenever the aerodynamic lift and moment of the blade reach their peak values, a noise pulse is generated and propagates to the far field. As the amplitudes of the fluctuations of C_L and C_M are similar, it is the higher mean lift and moment of the T1 blade that gives rise to a stronger noise generation in the far field, resulting in a noise amplitude 30% higher than that of the NACA 0012 airfoil.

4.3. NOISE DUE TO STRUCTURAL RESONANCE

For an elastic blade, the coupled structural response of the blade changes the aerodynamic forces experienced by the blade. Consequently, the fluid–blade interactions and the generated noise are altered. Conlisk [10] studied the acoustic pressure fluctuations when an inviscid discrete vortex impinges on a single-degree-of-freedom cylindrical bump

TABLE 1

Structural properties of the T1 blade

Parameter	E4
Blade chord c (m)	0·2
Blade mass m (kg/m)	0·094
Plunging stiffness K_h (N/m^2)	$2{\cdot}595 \times 10^6$
Pitching stiffness K_θ (N)	$1{\cdot}046 \times 10^5$
Moment of inertia I (kgm)	$7{\cdot}8 \times 10^{-4}$
Elastic axis a (% of chord)	45%
Center of gravity C.G. (% of chord)	37·5%
Bending natural frequency f_h (Hz)	833
Pitching natural frequency f_θ (Hz)	1875
f_h'—non-dimensional f_h	1·666
f_θ'—non-dimensional f_θ	3·75

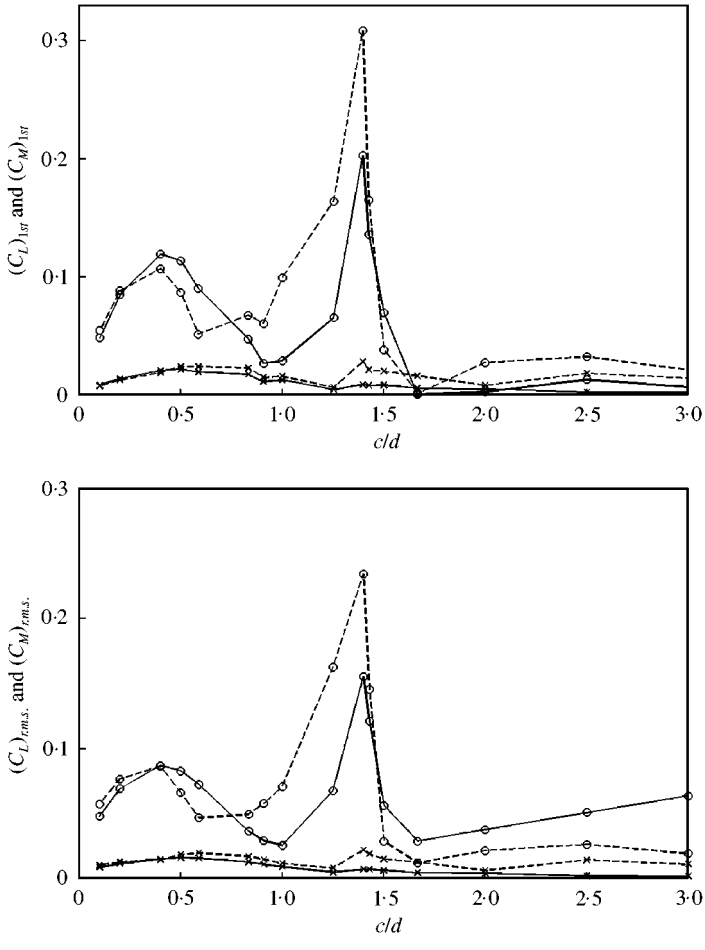

Figure 6. Variations of the first harmonic and root mean square values of the lift and moment coefficients, C_L and C_M, with c/d for elastic blade. ———, NACA 0012 airfoil; – – – – –, T1 blade. ○, C_L; ×, C_M.

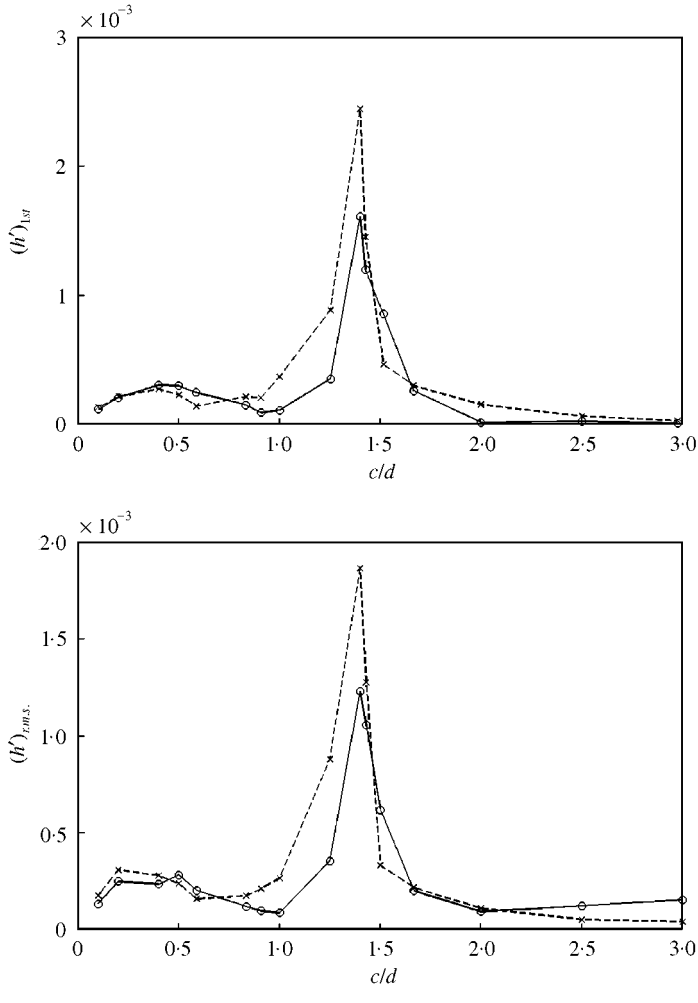

Figure 7. Variations of the first harmonic and root mean square values of the plunging displacement h with c/d for elastic blade. ———, NACA 0012 airfoil; – – – – –, T1 blade.

structure. The vortex approaches, interacts with the structure and noise is generated. After the vortex passes over the structure, if the structure is elastic, the structure is excited to vibrate and the fluid–structure interaction continues to radiate noise. However, in case of interaction with a rigid structure, the noise decays rapidly to zero. In an analysis of the impingement of a vortex on a single-degree-of-freedom elastic thin plate [24], the associated noise was found to depend critically on the ratio of the plate structural natural angular frequency to the vortex convection velocity divided by the vortex core size. If this ratio is greater than unity, the noise signature is dominated by fluctuations at the plate natural frequency. These observations clearly reveal that flow-induced vibrations not only modify the fluid–structure interaction but also the noise generation as well.

The aerodynamic and structural responses of the elastic NACA 0012 airfoil and the T1 blade under the same oncoming KVS excitations as in the rigid cases are computed using the same computational parameters. The time stationarity of the structural response and noise signature is fully achieved. The structural properties of a real-life turbine blade are

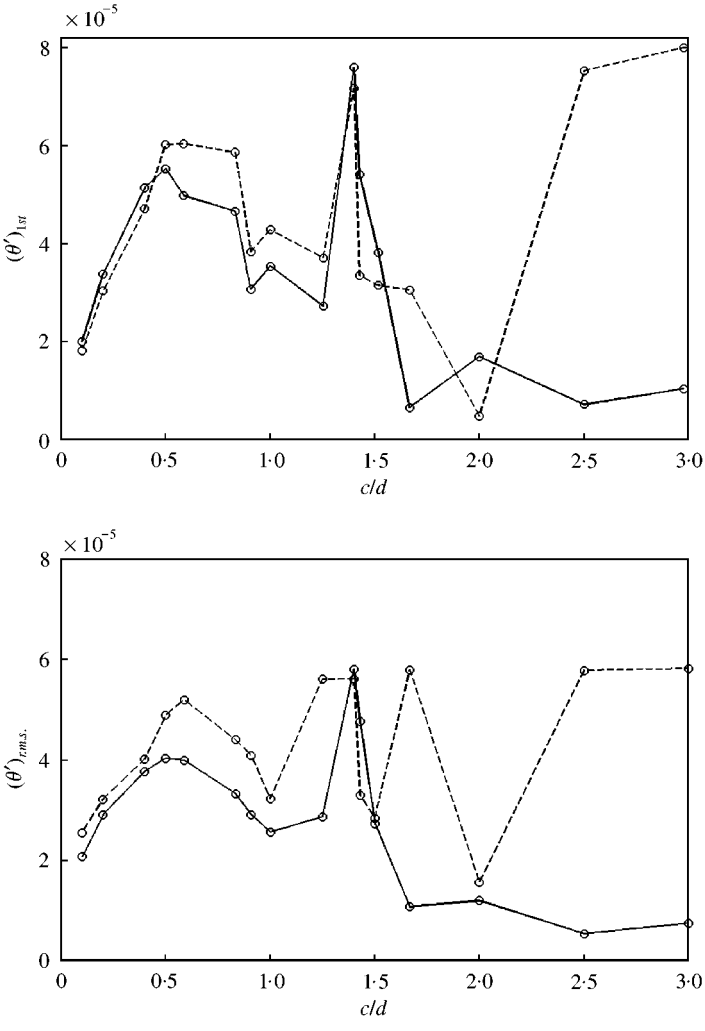

Figure 8. Variations of the first harmonic and root mean square values of the pitching displacement θ with c/d for elastic blade. ———, NACA 0012 airfoil; – – – – –, T1 blade.

adopted for the airfoil/blade, which belong to the type E4 in the study of So *et al.* [15], and are listed in Table 1. One may note that the bending and pitching frequencies f_h and f_θ, reported in the table correspond to the lowest natural frequencies in vacuo, i.e., the flow effect is ignored. These natural frequencies will be modified by the flow and will take different values in a coupled blade–vortex system.

The non-dimensional frequency parameter c/d of the KVS excitation was varied from 0·1 to 3. Figure 6 illustrates the distributions of the first harmonic, $(C_L)_{1st}$ and $(C_M)_{1st}$, and the root mean square, $(C_L)_{r.m.s.}$ and $(C_M)_{r.m.s.}$, values with respect to c/d. The results agree well with those reported by So *et al.* [15]. It can be seen that as a result of blade–vortex interactions, the peak aerodynamic response is now achieved at $c/d = 1{\cdot}4$, in addition to the fairly broad peak at the aerodynamic resonance at $c/d = 0{\cdot}5$. This reveals the occurrence of the structural resonance phenomenon [10]. It can be seen that the general resonance pattern is modified by the structural response of the blade and the fluid flow and the structural properties of the airfoil/blade interact to create a new dominant peak in the c/d

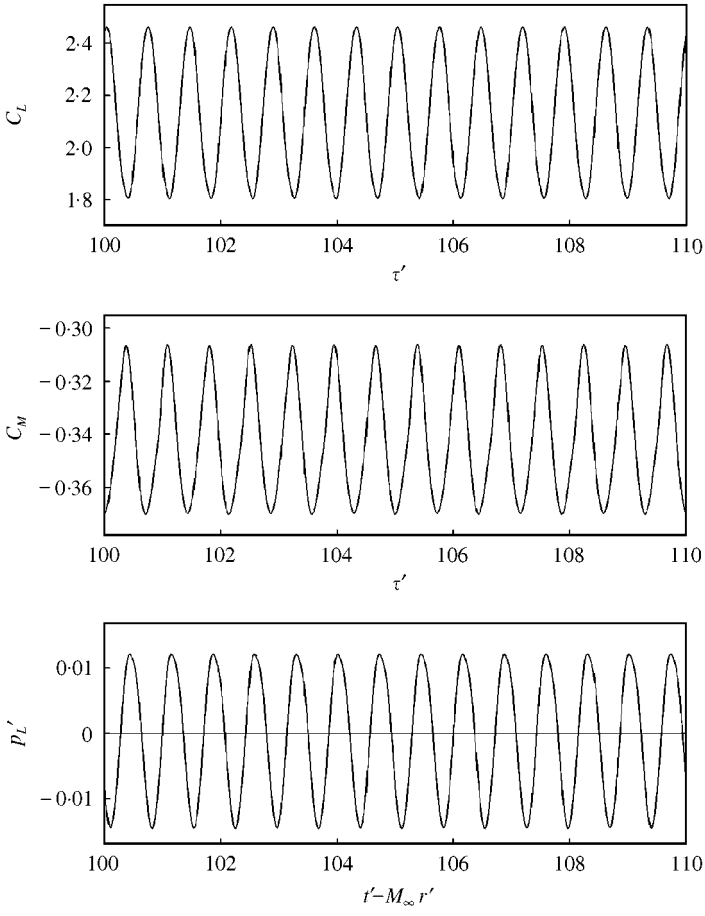

Figure 9. Time histories of the lift coefficient C_L, moment coefficient C_M and loading noise p_L' for the elastic T1 blade with $c/d = 1{\cdot}4$

distribution. In the present case, the new dominant peak occurs at $c/d = 1{\cdot}4$. Note that the dominant frequency of the coupled elastic blade–vortex system is close to the lowest bending frequency of 1·666 of the blade alone. The occurrence of resonance at the lowest bending frequency is further supported by the distributions of the normalized plunging and pitching displacements, h' (Figure 7) and θ' (Figure 8). The plunging displacement h displays a clear peak at $c/d = 1{\cdot}4$ whereas the latter just shows broad distributions of comparable magnitudes at $c/d = 0{\cdot}5$ and 1·4. It should be noted from these figures that, within the range of c/d investigated, the aerodynamic and structural responses of the T1 blade is stronger than that of the NACA 0012 airfoil due to the high loading characteristics of the T1 blade. However, their trends are rather independent of the geometry of the blade.

The noise signature in the far field of an elastic airfoil/blade consists of both loading and thickness components (equations (9) and (10)). The time histories of the normalized loading noise p_L' and thickness noise p_T' of the elastic T1 blade are illustrated in Figures 9 and 10, together with the aerodynamic coefficients C_L and C_M, and the plunging and pitching displacements, h' and θ'. Similar to the rigid blade, strong correlation between the aerodynamic coefficients and the loading noise is evident. The same correlation can be observed between the plunging and pitching displacements and the thickness noise. Figures

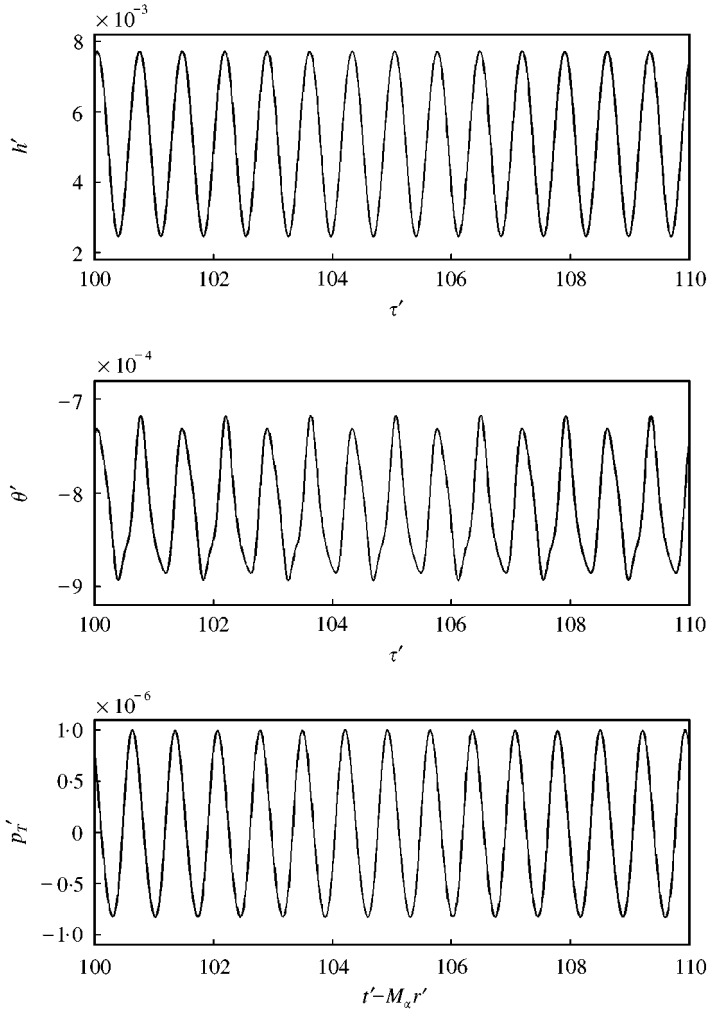

Figure 10. Time histories of the plunging amplitude h, pitching amplitude θ and thickness noise p'_T for the elastic T1 blade with $c/d = 1{\cdot}4$.

11 and 12 show the distributions of the first harmonic, $(p'_L)_{1st}$ and $(p'_T)_{1st}$, and the root mean square, $(p'_L)_{r.m.s.}$ and $(p'_T)_{r.m.s.}$, values with respect to c/d. Maximum noise generation occurs at $c/d = 1.4$. Compared with the maximum magnitude of the loading noise distributions in the rigid blade case (Figure 5), the elastic T1 blade has a 4·6–6·5 times increase in magnitude whereas the elastic NACA 0012 airfoil only increases by 3–4 times. The significant quantitative difference in the noise distributions suggests that the structural response effectively amplifies the loading noise generated in the far field. One should note that the structural response only gives rise to a doubling of the maximum magnitude of the lift and moment coefficient (Figures 4 and 6). The geometry of the blade, and thus the loading characteristics, seems to be an important factor that affects the noise generation. Further, the maximum values of the $(p'_L)_{1st}$ and $(p'_L)_{r.m.s.}$ of the T1 blade are approximately 52% higher than those of the NACA 0012 airfoil, whereas the distributions of the thickness noise, $(p'_T)_{1st}$ and $(p'_T)_{r.m.s.}$, of the NACA 0012 airfoil are weaker than the T1 blade by almost an order of magnitude.

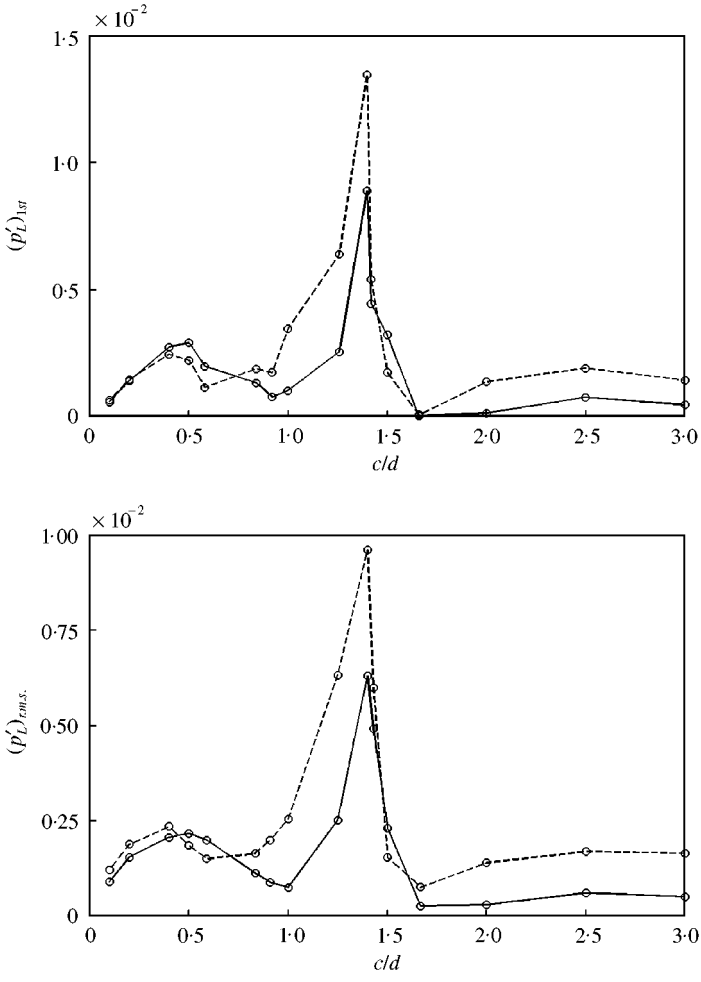

Figure 11. Variations of the first harmonic and root mean square values of the loading noise p'_L with c/d for elastic blade. ———, NACA 0012 airfoil; – – – – –, T1 blade.

Although an elastic blade is able to generate both loading noise and thickness noise, it is found that during the structural resonance of the present excited blade–vortex system, only the loading noise dominates in the far field, as evident in their spectra at $c/d = 0{\cdot}5$ and $1{\cdot}4$ (Figure 13). In general, the amplitude of p'_L is higher than that of p'_T by at least two orders of magnitude. This means that the loading noise power is four orders of magnitude stronger and thus the thickness noise due to blade vibrations is negligible in the far field. This is consistent with the arguments of Farassat *et al.* [18, 19] that as far as the acoustics is concerned, for a moving body in a low Mach number flow ($M_\infty \approx 0{\cdot}3$ in the present study), practically only the aerodynamic loading contributes to the noise. However, this does not necessarily mean that the structural response, albeit weak, can be ignored in the analysis of excited elastic blade–vortex interaction noise since the excited structural resonance of the blade could significantly modify the aerodynamic loading at structural resonance and consequently the associated loading noise. Only if the frequency of the oncoming vortices is far away from the resonance frequency, for instance $c/d < 1$ or $c/d > 2{\cdot}5$, the elastic blade exhibits similar aerodynamic responses to the corresponding blade (Figures 4 and 6) and gives similar farfield noise radiation (Figures 5 and 11).

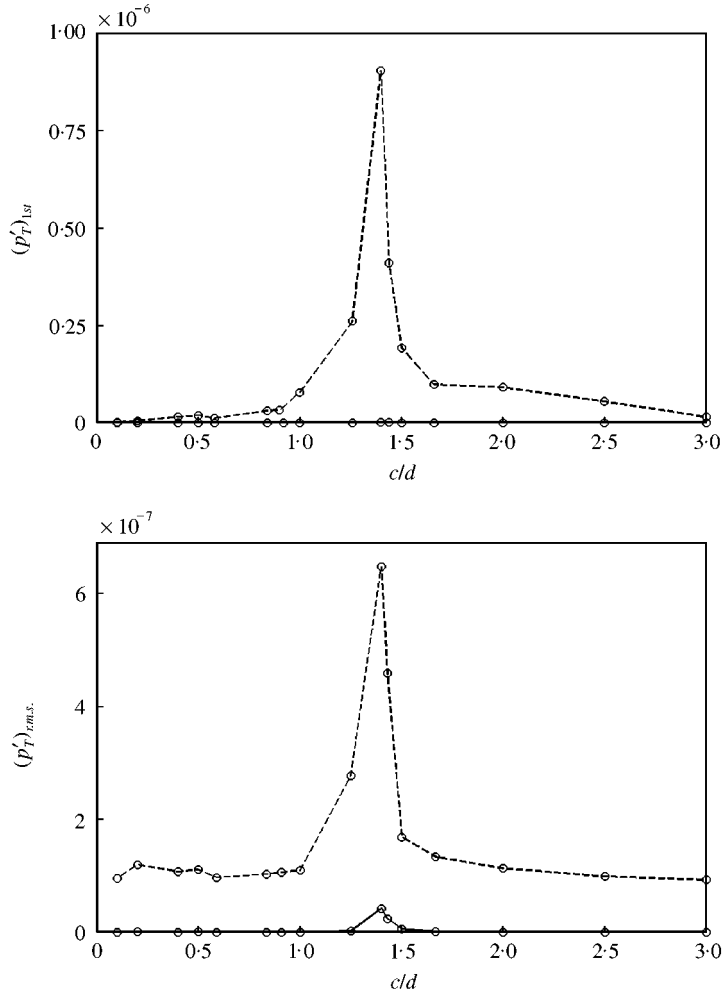

Figure 12. Variations of the first harmonic and root mean square values of the thickness noise p'_T with c/d for elastic blade. ———, NACA 0012 airfoil; – – – – –, T1 blade.

5. CONCLUSIONS

The influence of oncoming vortices in a uniform flow on the aerodynamic and structural responses of an airfoil/blade and its associated noise generation in the far field has been investigated. Due to its relevance to helicopter rotor and turbomachinery applications, the representative Karman vortex street (KVS) pattern has been used to simulate the upstream vortical excitations. A parameter related to the ratio of the chord length c to the vortex spacing d is of fundamental importance and its influence on the structural response of the airfoil/blade and the noise generation has been examined. Two types of airfoil/blade are considered, a NACA 0012 airfoil and a T1 turbine blade with high aerodynamic loading.

The oncoming flow is assumed to be inviscid and the flow around the blade remains attached to the blade surface. Aerodynamic effects and the noise generation due to the oncoming vortices are examined first by considering a rigid airfoil/blade. The results show that the magnitude of the aerodynamic response is decreasing with the frequency parameter

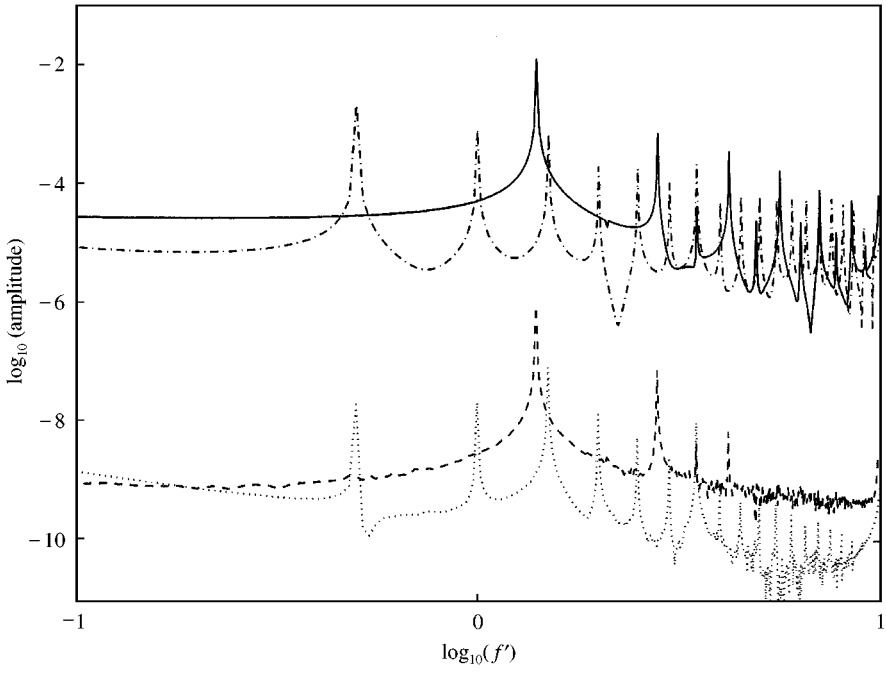

Figure 13. Spectra for the loading noise and thickness noise of the elastic T1 blades. ———, loading noise with $c/d = 1{\cdot}4$; –·–·–·–, thickness noise with $c/d = 1{\cdot}4$; – – – – – –, loading noise with $c/d = 0{\cdot}5$; ·····, thickness noise with $c/d = 0{\cdot}5$.

c/d. Aerodynamic resonance is observed at $c/d = 0{\cdot}5$, $1{\cdot}5$ and $2{\cdot}5$. In this situation, the aerodynamic loading is the only source of far field noise, which also attains dominant peaks at the same c/d values. Even though the high-loading T1 blade generates stronger noise than the NACA 0012 airfoil under the same oncoming excitation, the general far field noise trend is similar to that of the airfoil.

When the airfoil/blade under consideration is elastic, its aerodynamic and structural responses to the oncoming KVS vortices show some differences with the rigid case. In addition to the aerodynamic resonance peak at $c/d = 0{\cdot}5$, an exceptionally sharp peak, corresponding to the lowest bending mode of the structure, at $c/d = 1{\cdot}4$, emerges. This is resulted from the merging of the structural resonance with the aerodynamic resonance and happens with both the NACA 0012 airfoil and the T1 blade. The flow-induced vibrating blade generates loading noise and thickness noise in the far field. Both noise signature show a sharp peak at the same $c/d = 1{\cdot}4$ as a consequence of enhanced aerodynamic loading and vibration of the airfoil/blade. Though the thickness noise generated from the vibration of the airfoil/blade is negligible, an elastic airfoil/blade generates noise of different characteristics due to the change of the aerodynamic loading by the blade–vortex interaction.

ACKNOWLEDGMENTS

The authors would like to acknowledge support given to them by the Research Grants Council of the HKSAR under Grant No. PolyU5161/00E. Furthermore, funding support for the first author in the form of a Research Fellowship tenable at the Department of

Mechanical Engineering, The Hong Kong Polytechnic University is gratefully acknowledged.

REFERENCES

1. E. NAUDASCHER and D. ROCKWELL 1994 *Flow-Induced Vibrations. An Engineering Guide*. Rotterdam: A. A. Balkema.
2. G. PARKINSON 1989 *Journal of Fluids and Structures* **26**, 160–224. Phenomena and modeling of flow-induced vibrations of bluff bodies.
3. S. WIDNALL 1971 *Journal of the Acoustical Society of America* **50**, 354–365. Helicopter noise due to blade–vortex interaction.
4. W. R. SPLETTSTOESSER, K. J. SCHULTZ and R. M. MARTIN 1990 *American Institute of Aeronautics and Astronautics Journal* **28**, 593–600. Rotor blade–vortex interaction impulsive noise source localization.
5. J. C. HARDIN and S. L. LAMKIN 1987 *Transaction of the American Society of Mechanical Engineers, Journal of Vibration, Acoustics, Stress, and Reliability in Design* **109**, 29–36. An Euler code calculation of blade–vortex interaction noise.
6. J. C. HARDIN and S. L. LAMKIN 1987 *Journal of Aircraft* **24**, 120–125. Concepts for reduction of blade/vortex interaction noise.
7. F. OBERMEIER and K.-Q. ZHU 1993 *Journal of Aircraft* **30**, 81–87. Sound generation by rotor–vortex interaction in low Mach flow.
8. Y. H. YU, C. TUNG, J. GALLMAN, K. J. SCHULTZ, B. VAN DER WALL, P. SPIEGEL and B. MICHEA 1995 *Journal of Aircraft* **32**, 970–977. Aerodynamics and acoustics of rotor blade–vortex interactions.
9. D. R. POLING, L. DADONE and D. P. TELIONIS 1989 *American Institute of Aeronautics and Astronautics Journal* **27**, 694–699. Blade–vortex interaction.
10. A. T. CONLISK 1985 *Transaction of the American Society of Mechanical Engineers, Journal of Vibration, Acoustics, Stress, and Reliability in Design* **107**, 210–215. Computation of far-field sound generation in a fluid–structure problem.
11. S. A. T. STONEMAN, K. HOURIGAN, A. N. STOKES and M. C. WELSH 1988 *Journal of Fluid Mechanics* **192**, 455–484. Resonant sound caused by flow past two plates in tandem in a duct.
12. R. PARKER and S. A. T. STONEMAN 1989 *Proceedings of Institution of Mechanical Engineers. Part C. Journal of Mechanical Engineering Science* **203**, 9–19. The excitation and consequences of acoustic resonances in enclosed fluid flow around solid bodies.
13. M. J. LUCAS, R. S. NOREEN, L. C. SUTHERLAND, M. C. COLE III and M. C. JUNGER 1997 *Handbook of the Acoustic Characteristics of Turbomachinery Cavities*. New York: ASME Press.
14. J. M. FEIEREISEN, M. D. MONTGOMERY and S. FLEETER 1994 *Transaction of the American Society of Mechanical Engineers, Journal of Turbomachinery* **116**, 676–685. Unsteady aerodynamic forcing functions: A comparison between line theory and experiment.
15. R. M. C. SO, I. JADIC and M. P. MIGNOLET 1999 *Journal of Fluids and Structures* **13**, 519–548. Fluid–structure resonance produced by oncoming alternating vortices.
16. I. JADIC, R. M. C. SO and M. P. MIGNOLET 1998 *Journal of Fluids and Structures* **12**, 631–654. Analysis of fluid–structure interactions using a time-marching technique.
17. D. G. CRIGHTON 1975 *Progress of Aerospace Sciences* **16**, 31–96. Basic principles of aerodynamic noise generation.
18. J. E. FFOWCS WILLIAMS and D. L. HAWKINGS 1969 *Philosophical Transaction of Royal Society of London. Series A* **264**, 321–341. Sound generation by turbulence and surfaces in arbitrary motion.
19. F. FARASSAT and G. P. SUCCI 1983 *Vertica* **7**, 309–320. The prediction of helicopter discrete frequency noise.
20. F. FARASSAT and K. S. BRENTNER 1998 *Theoretical and Computational Fluid Dynamics* **10**, 155–170. The acoustic analogy and the prediction of the noise of rotating blades.
21. J. E. FFOWCS WILLIAMS and D. L. HAWKINGS 1968 *Journal of Fluid Mechanics* **31**, 779–788. Shallow water wave generation by unsteady flow.
22. S. K. TANG and J. E. FFOWCS WILLIAMS 1999 *Acustica* **84**, 1007–1013. Acoustic radiation from a vortex approaching a circular cylinder with surface suction.
23. M. S. HOWE 1984 *IMA Journal of Applied Mathematics* **32**, 187–209. On the absorption of sound by turbulence and other hydrodynamic flows.
24. M. S. HOWE 1994 *Journal of Sound and Vibration* **177**, 325–336. Elastic blade–vortex interaction noise.

25. H. P. HODSON and W. N. DAWES 1998 *Transaction of the American Society of Mechanical Engineers, Journal of Turbomachinery* **120**, 276–284. On the interpretation of measured profile losses in unsteady wake — Turbine blade interaction studies.
26. K. FUNAZAKI and T. NISHIYAMA 1989 in *Unsteady Aerodynamics and Aeroelasticity of Turbomachines and Propellers*, Proceedings of the 5th International Symposium, 287–300. Measurements of simulated wake/rotor interaction phenomena in turbomachinery.
27. I. H. ABBOTT and A. E. VON DOENHOFF 1959 *Theory of Wing Sections*. New York: Dover.